Thin Solid Films 531 (2013) 172–178

Contents lists available at SciVerse ScienceDirect

Thin Solid Films

journal homepage: www.elsevier.com/locate/tsf

Structural mosaicity and electrical properties of pyrolytic SnO_2:F thin films

F.A. Garcés [a,*], N. Budini [a], R.R. Koropecki [a,b], R.D. Arce [a,b]

[a] Instituto de Desarrollo Tecnológico para la Industria Química, UNL-CONICET, Güemes 3450, S3000GLN Santa Fe, Argentina
[b] Facultad de Ingeniería Química, UNL, Santiago del Estero 2829, S3000AOM Santa Fe, Argentina

ARTICLE INFO

Article history:
Received 3 April 2012
Received in revised form 19 December 2012
Accepted 14 January 2013
Available online 20 January 2013

Keywords:
Mosaicity
Sol–Gel
Spray deposition
Tin dioxide
Transparent conducting oxide
X-ray diffraction

ABSTRACT

In this work we present structural and electrical properties of SnO_2:F thin films deposited on glass substrate by the spray pyrolysis technique. The precursors of SnO_2:F were synthesized by a sol–gel method, starting from a $SnCl_4 \cdot 5H_2O$/ethanol mixture and using NH_4F/H_2O as a dopant. Different properties were observed depending on the deposition time of the films. The structural characteristics of the layers, like crystal size, preferential growth orientation and mosaicity, were studied by X-ray diffraction. These results were compared and correlated with those obtained from electrical measurements, such as carrier density, Hall mobility and resistivity. We have found that for longer deposition times, the mosaicity of the crystallites increases. This process is accompanied by a decrease in the resistivity.

© 2013 Elsevier B.V. All rights reserved.

1. Introduction

Tin oxide (SnO_2) is one of the most interesting transparent conducting oxides (TCO) since it combines high transparency in the visible region of the electromagnetic spectrum with a high electrical conductivity. This makes it widely applicable in a variety of optoelectronic devices [1–3]. SnO_2 deposition can be carried out by different methods, such as chemical vapor deposition [4], reactive sputtering [5] and spray pyrolysis [6]. The latter technique is considered as the most appropriate in many areas for the deposition of TCO layers, since it requires minimal costs to be implemented and allows obtaining films with high optical and electrical qualities. The spray pyrolysis method is simple and applicable to large area depositions. Besides this, the deposition can be carried out at atmospheric pressure, which is also advantageous.

Since oxides are insulators in their intrinsic state, they have to be doped in order to make them suitable for electronic transport. Typical dopants for SnO_2 are fluorine (F), chlorine (Cl) and antimony (Sb). Among these options, the fluoride ion is preferred because the doped films exhibit high transparency and good electrical conductivity. These F-doped films are also very attractive due to their good adherence to polycrystalline and amorphous substrates such as glass, metals and oxides.

Several reports on doped SnO_2 thin films focus their results on the variation of electrical and structural properties with deposition temperature and dopant concentration [6–13]. However, there are scarce studies concerning the influence of thickness on their electronic transport and structural properties [14–18].

In this context, we present results obtained for SnO_2:F samples synthesized by the sol–gel method and deposited by spray pyrolysis, as a function of deposition time (i.e. varying thickness). The optical and morphological characterizations of the films were carried out by optical interferometry (transmittance and reflectance), X-ray diffraction (XRD), scanning electron and atomic force microscopies (SEM and AFM). In turn, the electrical characterization was performed by means of Hall effect measurements, which provided the resistivity, the mobility and the dopant concentration of the films. The correlation between these parameters and the effect of thickness on morphology and transport properties is discussed.

2. Experimental details

The precursor solution was synthesized from Sn(IV) salts, using $SnCl_4 \cdot 5H_2O$. A 0.2327 M solution was prepared in a mixture of polar solvents: CH_3CH_2OH 99.9% and deionized H_2O in a ratio of 6:1, respectively. We used 0.163 g of NH_4F as the dopant source, to obtain a concentration of 5 wt.% of F with respect to the amount of Sn present in the stock solution, i.e. making a F/Sn = 0.05 relation. The choice of this concentration was based on the optimization of optical and electrical properties. Subsequently the ethanolic solution was heated at 60 °C for 60 min to hydrolyze the Sn^{+4} ion and, in this way, obtain the $Sn(OH)_x$ solution. This precursor solution was deposited onto glass substrates using a spray pyrolysis system. The configuration scheme of this system has been reported by Gottlieb et al. [19]. The deposition temperature, controlled within ±2 °C, was set to 380 °C and the deposition times were in the range from 5 to 30 min.

We measured XRD patterns in the typical θ–2θ Bragg–Brentano configuration to look for the presence of SnO_2 characteristic peaks,

* Corresponding author. Tel.: +54 342 4559174; fax: +54 342 4550944.
E-mail address: fgarces@intec.unl.edu.ar (F.A. Garcés).

0040-6090/$ – see front matter © 2013 Elsevier B.V. All rights reserved.
http://dx.doi.org/10.1016/j.tsf.2013.01.020

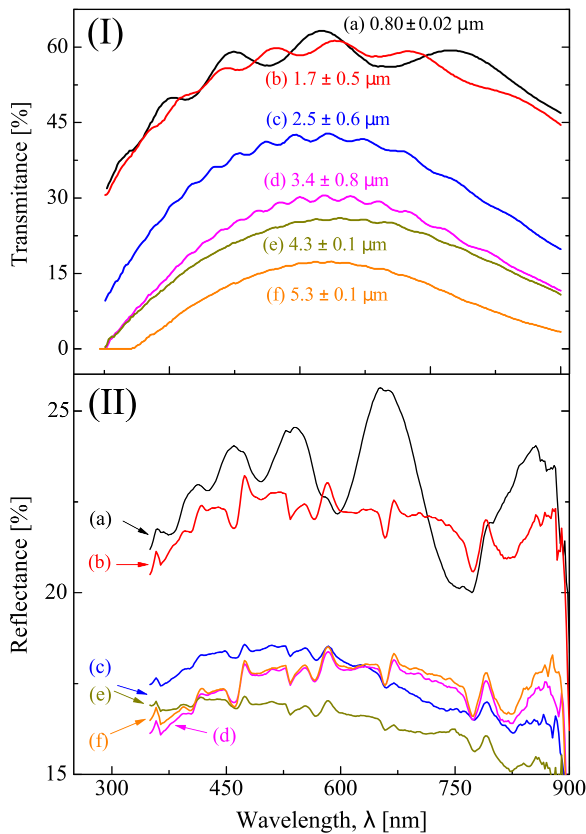

Fig. 1. (I) Transmittance and (II) reflectance spectra of SnO_2:F thin films, with a F concentration of 5%, prepared with different deposition times. The corresponding deposition times are: (a) 5 min; (b) 10 min; (c) 15 min; (d) 20 min; (e) 25 min; and (f) 30 min. The thickness of each film is indicated in figure (I).

in order to prove the existence of crystalline domains in the films. The patterns were normalized to account for thickness differences between samples. Structural mosaicity, or tilting between crystalline domains (explained below in more detail), was also calculated from XRD measurements. This was accomplished by rocking the incidence angle (θ) in 2° steps and the diffraction angle (2θ) around the peak maximum, centered at (θ_{hkl}, $2\theta_{hkl}$). Here, (hkl) are the Miller indices of the corresponding diffracting plane. This configuration and procedure has been reported by B. Marty et al. [20]. The diffraction patterns were subsequently integrated over the 2θ range to obtain the rocking curves as a function of $\Delta\theta$ ($=\theta-\theta_{hkl}$), whose width measures directly the degree of mosaicity.

The XRD patterns were obtained in a SHIMADZU XD-D1 diffractometer, operating with the Cu K_α line ($\lambda = 1.541$ Å). Direct transmittance and ultraviolet (UV) total reflectance (specular + diffuse) were obtained in a Shimadzu UV3600 spectrometer, using an integrating sphere under low angle incidence conditions for the latter case. AFM and SEM images were acquired in a NANOTEC probe system and in a JEOL JSM-35C electron microscope, respectively. The electron microscope was operated at 20 kV. Hall effect measurements were performed at room temperature, using the Van der Pauw method.

3. Results and discussion

Fig. 1 shows optical transmittance and reflectance data of the SnO_2:F films in the 350–900 nm range, for different deposition times. It is possible to observe a decreasing transmittance as the deposition time increased. For 5 and 10 min, the transmitted intensity reached a value of around 65%. Similarly, the total reflectance for these times was around 25% and decreased to about 14% for longer deposition times. This abrupt decrease of film reflectance for higher deposition times is attributed to morphological changes evidenced from XRD patterns, which will be discussed later.

By extending the deposition time, the maximum transmittance decreased from ~45% (for 15 min) to ~17% (for 30 min). This reduction is attributed to optical scattering induced by changes in the film morphology, which we will also discuss shortly.

By using the optical thickness in the transmittance spectra, and taking the refractive index as a constant (n~2) in the wavelength range between 350 and 900 nm [21], we used the following expression to obtain the thickness dependence on the deposition time [22]

$$nd = \frac{k\lambda_1\lambda_2}{2(\lambda_1-\lambda_2)}, \quad (1)$$

where λ_1 and λ_2 represent the wavelengths corresponding to two maxima or two minima of the transmittance spectrum and k is the number of maxima or minima in the selected range of wavelengths (λ_1, λ_2). In this way, we have calculated the thickness of the deposited SnO_2:F films, which are indicated in Fig. 1.

Fig. 2(a) and (b) shows SEM images of a sample deposited during 15 min at 380 °C, as described in the Experimental details section. Fig. 2(a) is a cross-sectional image of the film (right side) and the glass substrate (left side). The film presented a uniform thickness along the scanned area. We have measured the thickness in different regions of the film in order to confirm its uniformity. Therefore, thickness values determined from SEM images can be used to confirm those values calculated with Eq. (1). This also allowed us to determine the thickness of thicker samples (deposited in 25 and 30 min), for which it was difficult to distinguish maxima and minima in the transmittance spectra.

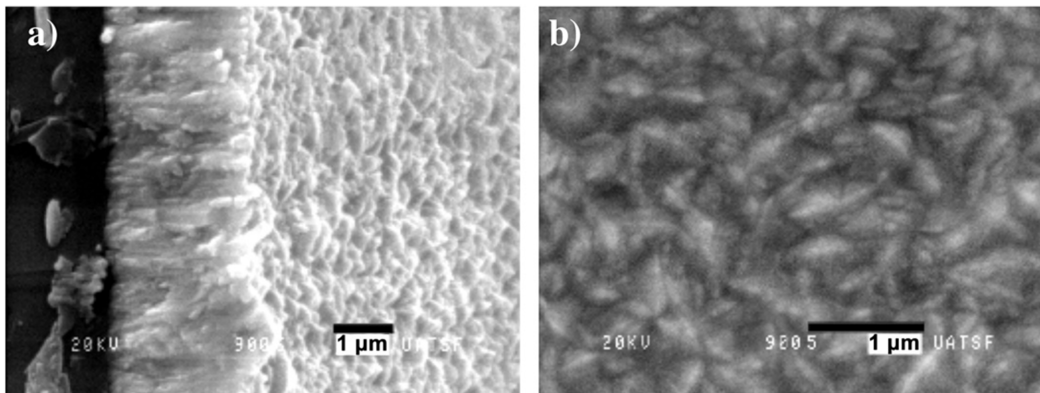

Fig. 2. SEM images of a SnO_2:F layer with a thickness of 2.7 μm. View of (a) the cross section and (b) the surface.

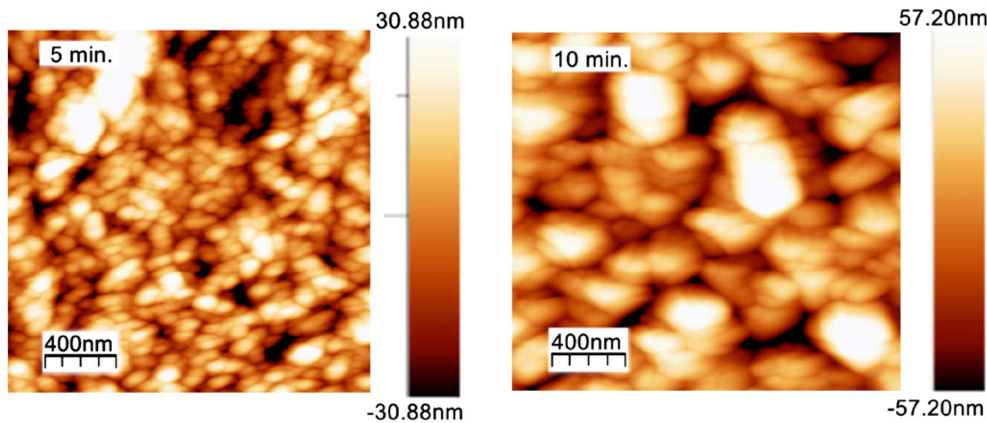

Fig. 3. AFM images of SnO_2:F layers deposited on glass for two different deposition times (5 and 10 min).

In turn, Fig. 2(b) shows the surface of the film and reveals a high density of elongated structures throughout the examined area. Such structures have been reported by Agashe et al. [18] for thicker films. The morphology observed is attributed to the fact that grains oriented in the [2 0 0] direction prevail over those grown in other orientations, allowing the development of these structures. This suggests a preferential grain orientation during growth.

Fig. 3 presents the AFM images obtained for two samples with thicknesses greater than 500 nm, deposited on glass substrates with different deposition times. As we have mentioned previously, an increase in the film thickness resulted in significant morphologic changes. In particular, as thickness increased, we observed both an increase in surface roughness and grain size, as shown in Fig. 4. The roughness and grain size determined from AFM images, for films deposited in 5 min, were 14 nm and 73 nm, respectively. By increasing the deposition time to 10 min we obtained larger values of 28 nm and 122 nm, respectively.

The variation of thickness as a function of deposition time followed a linear trend between 5 and 15 min. The obtained values were in accordance to those reported by other authors [9,10]. Also, in this range the surface roughness suffered a sudden increment before decreasing slowly for longer deposition times (>15 min). Although surface roughness decreased slightly between 15 and 30 min, we consider that the difference between the corresponding values (of about 4 nm) is negligible. However, there is an important increment in both roughness and grain size between deposition times of 5 and 10 min. By observing the

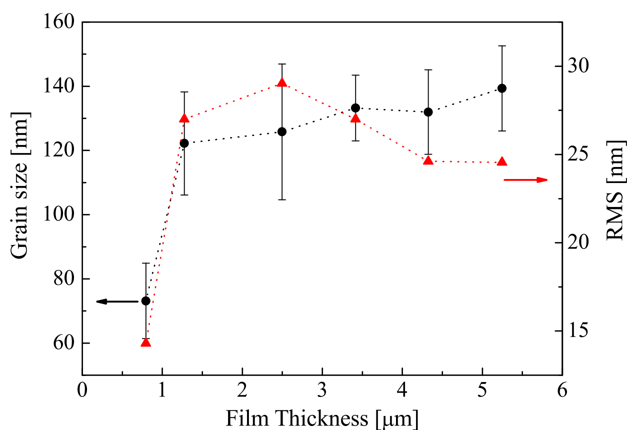

Fig. 4. Variation of grain size (circles) and roughness (triangles) of SnO_2:F/glass layers as a function of film thickness. Solid lines are only a guide to observe the trend of experimental data.

reflectance spectra of these samples (Fig. 1) it seems natural to attribute the loss of interference in the reflectance spectrum of the 10 min sample to this jump in roughness. Also, the absence of interference in the reflectance spectra for longer deposition times can be explained by the same argument, since roughness kept almost constant.

Therefore, the information gathered from the surface study allowed concluding that for lower deposition times the grains have an ovoid shape (Fig. 3). Also, an increase in film thickness leads to a change in morphology, giving as a result larger structures. This effect could be attributed to the nucleation of small structures, after short deposition times, and their subsequent agglomeration to form larger and more stable structures for longer deposition times.

As is shown in the XRD patterns of Fig. 5, FTO layers deposited during 5 min and 10 min had a preferential orientation in the [2 0 0] direction. For longer deposition times the orientation in the [2 0 0] direction decreased until it disappeared [16], but the [2 1 1] direction remained and decreased slowly as the deposition time increased. This texture change from a [2 0 0]-oriented to a [2 1 1]-oriented film explains why the transmittance is optimal for lower thicknesses. Also, this sorts out the fact that reflectance dropped abruptly for samples deposited during 15 min or more (Fig. 1), in which the preferential orientation changed from the [2 0 0] to the [2 1 1] direction.

The XRD patterns also reveal the polycrystalline nature of the films. Moreover, the observed peaks are coincident with those of the cassiterite phase (reference 1-072-1147, reported in the ICSD database), shown as vertical solid lines in Fig. 5. This indicates the presence of the tetragonal phase of SnO_2 with preferential orientation in the [2 0 0] direction. Other crystalline directions, such as [1 0 1] and [2 1 1], are present for all deposition times, except for 30 min where both directions diffract with low intensity. The intensity of the [1 1 0] direction, corresponding to 100% in the ICSD database, is nearly zero in our samples and overlaps with noise level.

On the other hand, the peaks marked with asterisks (*) belong to secondary phases which were favored as thickness increased. Such is the case of $(Sn_2O_2F)Sn_2$ and SnO peaks located at $2\theta = 31.3°$ and 29.9°, respectively [23]. For a deposition time of 15 min or higher, the intensity of the [2 0 0] direction, initially marked as preferential, decreased. Also, the intensities of the (1 0 1) and (2 1 1) peaks are reduced, evidencing a loss of these orientations as thickness increased. Moreover, for these deposition times the (2 1 1) peak appeared as preferential, showing a particularly strong orientation for 15 min.

Due to the behavior observed in the structure of the films, we performed measurements to analyze the homogeneity of the material. The rocking curves around the diffraction angle of maximum intensity were obtained as described in the Experimental details section [24,25].

In Fig. 6 we present the contour maps obtained for each film. These maps correspond to the SnO_2 characteristic (2 1 1) diffraction peak,

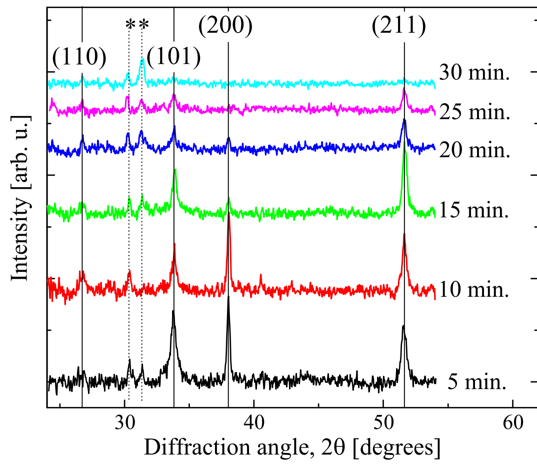

Fig. 5. XRD patterns of SnO_2:F films deposited on glass, with different deposition times.

since it is present in all samples (see Fig. 5). These rocking maps were acquired by varying the incidence angle between 5° and 47° in steps of 2° and scanning along 2θ between 50° and 53°. For deposition times of 5 and 10 min an intense (2 1 1) peak is seen at $2\theta=51.56°$, which is better defined and more intense for 10 min. In turn, for the 5 min sample the dispersion along 2θ is slightly broader than for 10 min.

The contour maps of the samples with deposition times longer than 10 min, show a splitting of the (2 1 1) peak for incidence angles between 10° and 43°. This indicates a loss of the initial orientation for thicker films. This is attributed to dislocations in the structure, caused by the generation of grain boundaries and the subsequent deformation of the next layer during deposition.

In Fig. 7 we present the rocking curves corresponding to the (2 1 1) peak for all samples as a function of the deposition time.

Fig. 7 shows the rocking curves corresponding to 5 and 10 min (top row). It is possible to see larger full-width at half-maximum (FWHM) values with respect to those obtained in epitaxial SnO_2

Fig. 6. Contour maps (θ, 2θ) of XRD patterns of films deposited on glass for different deposition times. The graphs are centered at the SnO_2 (2 1 1) peak position, $2\theta=51.63°$ and $\theta=2\theta/2=25.82°$.

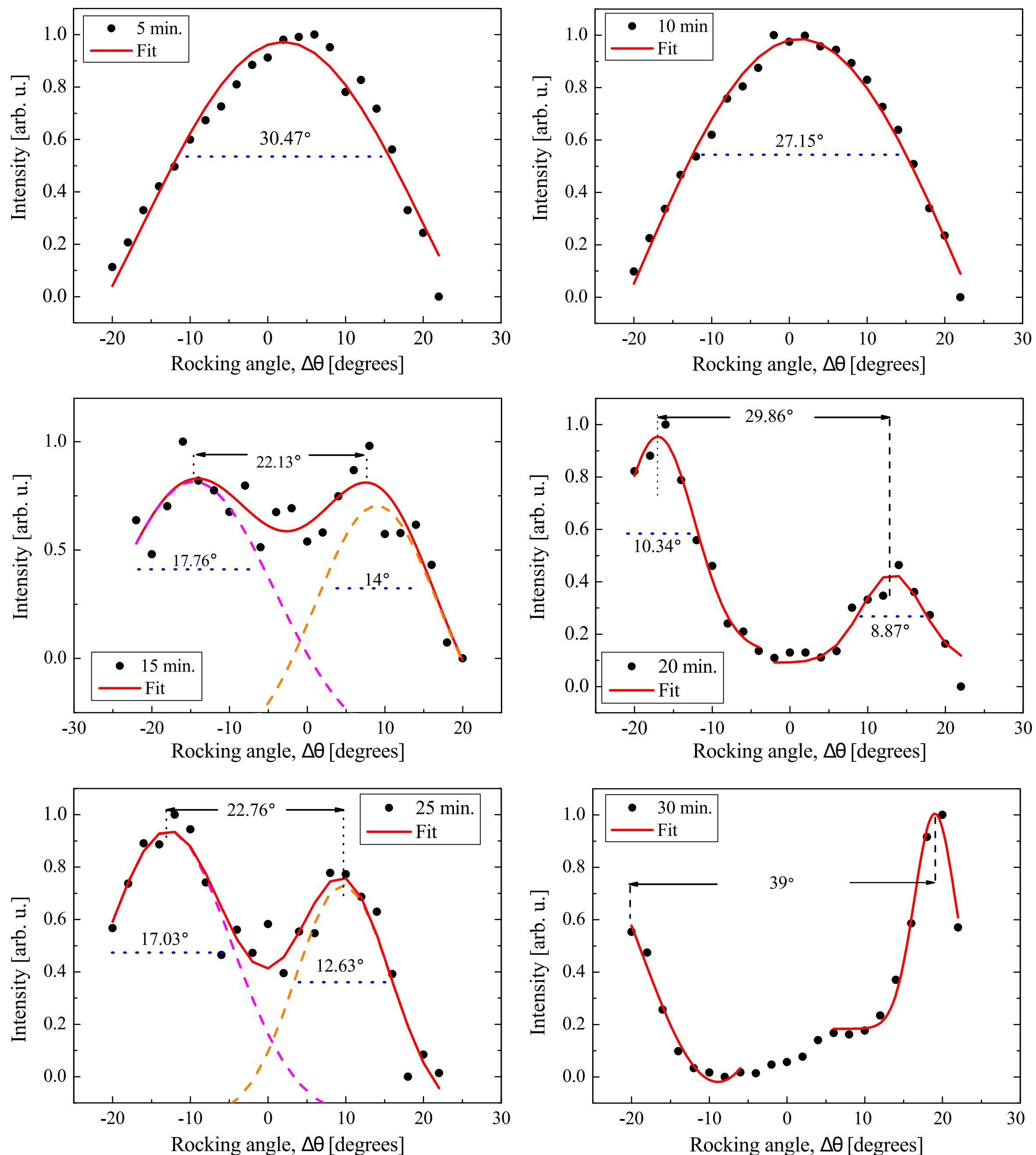

Fig. 7. Rocking curves, obtained for films with different deposition times: 5 min, 10 min, 15 min, 20 min, 25 min and 30 min. We chose the (2 1 1) diffraction peak of the XRD pattern, centered on $2\theta = 51.63°$ and $\theta = 2\theta/2 = 25.82°$. The solid lines are well fitted (Gaussian fit) to experimental data points (filled circles).

samples by Lee et al. [26,27]. They have reported values of 8° and 1.6°, respectively, and also mentioned that those values represent a low ratio in the lateral epitaxial material [28]. It is worth noting that higher FWHM values, as obtained in this work, indicate that the crystal growth mechanism in our films differs from an epitaxial growth and gives as a result a textured polycrystalline material [16]. On the other hand, for deposition times of 15 min and higher, different intensity distributions are observed along the $\Delta\theta$ axis. We attribute these distributions to misorientation or tilting between the same (2 1 1) plane of different crystalline domains, which caused the observed peak splitting. This evidences that different crystalline domains were formed, having dissimilar orientations from each other, giving place to what is called mosaicity. Thus, the mosaicity of the material may be directly quantified by this misorientation or tilting angle of a few degrees between different crystalline domains, separated by grain boundaries [27,29,30]. In this sense, a lower mosaicity corresponds to a more perfect crystalline structure.

To proceed with the analysis, the rocking curves were fitted using Gaussian functions according to Refs. [26] and [27]. As seen after inspecting the 15 min curve (Fig. 7, middle row left), there are two peaks separated by an angular distance of 22.13° which is a direct measure of mosaicity. At the same time, the FWHM values of both peaks are 17.76° and 14°, respectively, and quantify the mosaicity dispersion. The (2 1 1) peak splitting becomes more evident in the rocking curves obtained for deposition times of 20, 25 and 30 min (Fig. 7, middle row right and bottom row, respectively). Also, we observed that the intensity distribution possessed different magnitudes and widths, showing that crystalline domains are not statistically oriented in the same directions for different deposition times. However, there is a general trend or predisposition to a greater misorientation between crystalline domains for

longer deposition times. In our case, where the resulting films presented a polycrystalline nature, the mosaicity gives place to crystalline texture or roughness [16].

In XRD patterns (Fig. 5) we could identify secondary oxide phases (labeled with asterisks). They seem to reduce the tin oxide phase fraction, since oxyfluoride type compounds can form during film growth when a large amount of fluorine vapor is present in the pyrolysis zone (case of solutions containing large fluorine contents) or when the film is exposed for a long time to this vapor (case of thick films, typically thicker than 1 μm) [23]. These secondary phases between layers are known to "reset" the oriented growth and allow the formation of new nucleation sites, which cause a reorientation of the next tin oxide layer [31]. In Fig. 6, for deposition times beyond 10 min, we could see additional broad peaks in the XRD θ scan of the thicker samples, coming from reoriented new layers grown during deposition.

The presence of secondary phases in our films may originate strain, which can induce the development of a mosaic structure during deposition. As films grow with subsequent layers being slightly misoriented, neighboring grains begin to collide, resulting in a potentially increased internal stress. Typically, a mechanical system can withstand considerable stress by non-plastic deformations. However, after a deposition time of 15 min, the films seemed to reach a non-recoverable strain which caused the material to cede, giving as a result a textured material [32]. We conclude that there is a critical thickness (achieved after a deposition time of 15 min) in our films for which the internal stress is relieved through the formation of a mosaic structure.

The variation of sheet resistance and resistivity of the films as a function of thickness is shown in Fig. 8. Sheet resistance values decreased from 32 to 3.1 Ω/□ for thicknesses between 0.795 and 5.250 μm. Similarly, resistivity decreased from 3.1×10^{-3} to 1×10^{-3} Ω cm for thicknesses in the range from 0.795 to 1.280 μm, respectively. However, resistivity values did not vary significantly for higher thicknesses and remained almost constant. A value of 1.6×10^{-3} Ω cm was obtained for the largest thickness of 5.250 μm. The behavior observed for sheet resistance data is in accordance with that of grain size (see Fig. 4), which clearly increased up to 15 min of deposition time while the former decreased accordingly. For longer deposition times, the grain size presented a slight increment which was also followed by a consistent sheet resistance diminution. At the same time, the resistivity values diminished abruptly for deposition times up to 15 min and then remained almost constant. However, we attribute the slight increase observed in resistivity values for deposition times of 25 and 30 min to the higher degree of mosaicity (i.e. disorder) in these samples.

The variation of carrier concentration (n) and Hall mobility (μ) as a function of film thickness is shown in Fig. 9. We observed an almost linear dependence of carrier mobility as a function of film thickness.

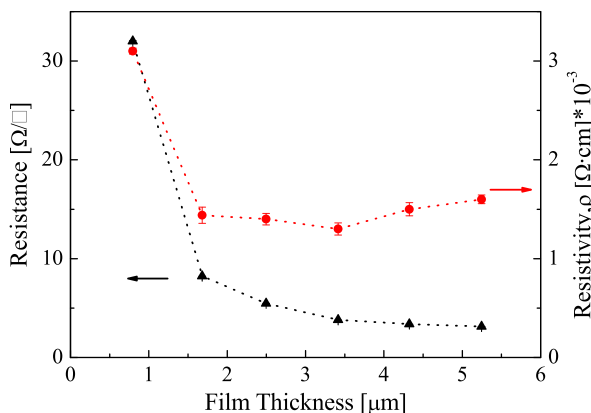

Fig. 8. Sheet resistance and resistivity of the films as a function of thickness. Solid lines are only a guide to observe the trend of experimental data.

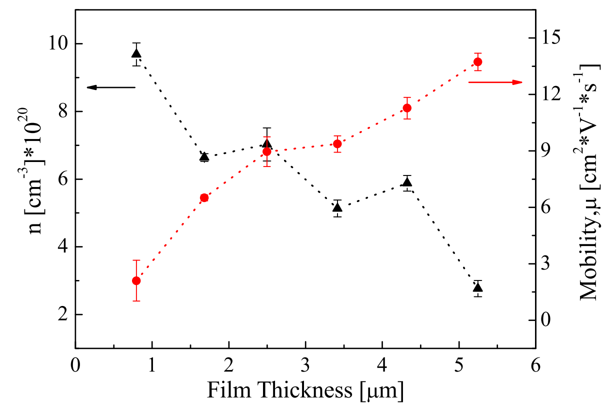

Fig. 9. Variation of volume carrier density (filled circles) and Hall mobility (open circles) as a function of film thickness. Solid lines are only a guide to observe the trend of experimental data.

As noted in the mosaicity contour maps of Fig. 6, as the deposition time increased the occurrence of crystalline mosaicity is more evident. Thus, the inclination between crystalline domains is higher and the structure results less strained. A less strained medium is known to present a lower density of scattering centers for charge carriers, allowing a higher mean free path and consequently extending the carriers lifetime before recombination. Therefore, despite the fact that mosaicity is related to a higher degree of disorder in the material, it also allows the material to release internal strain. Hence, we attribute the increment of carrier mobility with deposition time to the lower level of internal strain due to the higher degree of mosaicity in the films.

The values obtained for n are consistent with those reported in other works [12,14], ranging from 9.6×10^{20} to 2.8×10^{20} cm^{-3} for thicknesses between 0.795 and 5.250 μm, respectively. This gradual decrease of carrier concentration for thicker films has been mentioned previously by Elangovan et al. [17], and it is attributed to several factors such as morphology, roughness, composition and film/substrate interface. We consider that the reduction of carrier concentration with thickness may be also attributed to charge trapping at Sn(II) surface sites in grain boundaries [33], since these sites are likely to form dangling bonds. In particular, we have detected the presence of Sn(II) compounds for larger thicknesses. The formation of grain boundaries is attributed to misorientation or mosaicity between crystalline domains.

From the previous analysis of rocking curves, and their variation with deposition time (Fig. 7), we can validate the behavior of carrier concentration. The emergence of two different orientations of crystalline domains after a deposition time of 15 min, and the tilting between them, allows the formation of structural domains. In this way, for the highest deposition time (30 min) there is a grater mosaicity and, therefore, the carrier concentration is considerably affected by an increase of the crystalline texture.

4. Conclusion

We have obtained SnO_2:F thin films on glass through sol–gel synthesis and spray pyrolysis deposition. We showed the variation of some morphological characteristics, such as grain size and roughness, with film thickness. Also, we have correlated parameters like grain size and crystal domain orientation with deposition time by analyzing structural mosaicity. In all films, we have obtained resistivities in the order of 10^{-3} Ω cm and Hall mobilities of about 13.5 cm^2 V^{-1} s^{-1}. It has been found that by increasing the deposition time, the tilting between crystalline domains is greater. This has a direct influence on resistivity and carrier concentration. At this respect, we attributed the diminution of carrier concentration to the appearance of grain boundaries, which is induced by both the formation of crystalline domains and the increase of crystalline texture with thickness.

Acknowledgments

This work was partially supported by ANPCyT (project PICT 32515) and by the Universidad Nacional del Litoral (project CAID 2009 no 68-343). We also want to acknowledge the technical support of Ramón Saavedra.

References

[1] E. Comini, G. Faglia, G. Sberveglieri, Sens. Actuators, B 76 (2001) 270.
[2] T. Kamiya, H. Hosono, Int. J. Appl. Ceram. Technol. 2 (4) (2005) 285.
[3] S. Taniguchi, M. Yokozeki, M. Ikeda, T.-k. Suzuki, Jpn. J. Appl. Phys., Part 1 50 (2011) 04DF11.
[4] D. Calestani, M. Zha, A. Zappettini, L. Lazzarini, G. Salviati, Mater. Sci. Eng., C 25 (2005) 625.
[5] Y. Muto, N. Oka, N. Tsukamoto, Y. Iwabuchi, H. Kotsubo, Y. Shigesato, Thin Solid Films 520 (2011) 1178.
[6] Chin-Ching Lin, Mei-Ching Chiang, Yu-Wei Chen, Thin Solid Films 518 (2009) 1241.
[7] Chanchana Thanachayanont, Visittapong Yordsri, Chris Boothroyd, Mater. Lett. 65 (2011) 2610.
[8] Agus Purwanto, Hendri Widiyandari, Arif Jumari, Thin Solid Films 520 (2012) 2092.
[9] D. Zaouk, Y. Zaatar, A. Khoury, C. Llinares, J.-P. Charles, J. Bechara, Microelectron. Eng. 5 (1/52) (2000) 627.
[10] A.V. Moholkar, S.M. Pawar, K.Y. Rajpure, C.H. Bhosale, J.H. Kim, Appl. Surf. Sci. 225 (2009) 9358.
[11] Minoru Oshima, Kenji Yoshino, J. Electron. Mater. 3 (9/6) (2010) 819.
[12] E. Elangovan, K. Ramamurthi, J. Optoelectron. Adv. Mater. 5 (1) (2003) 45.
[13] M. Girtan, A. Bouteville, G.G. Rusu, M. Rusu, J. Optoelectron. Adv. Mater. 8/1 (2006) 27.
[14] Mikko Utriainen, Hanna Lattu, Heli Viirola, Lauri Niinistö, Roland Resch, Gernot Friedbacher, Mikrochim. Acta 133 (2000) 119.
[15] Chitra Agashe, Shailaja Mahamuni, Thin Solid Films 518 (2010) 4868.
[16] Chang-Yeoul Kim, Doh-Hyung Riu, Thin Solid Films 519 (2011) 3081.
[17] E. Elangovan, M.P. Singh, K. Ramamurthi, Mater. Sci. Eng., B 113 (2004) 143.
[18] Chitra Agashe, J. Hüpkes, G. Schöpe, M. Berginski, Sol. Energy Mater. Sol. Cells 93 (2009) 1256.
[19] B. Gottleb, R. Koropecki, R. Arce, R. Crisalle, J. Ferron, Thin Solid Films 199 (1991) 13.
[20] B. Marty, P. Moretto, P. Gergaud, J.L. Lebrun, K. Ostolaza, V. Ji, Acta Mater. 45 (1997) 791.
[21] J.P. Chatelon, C. Terrier, J.A. Roger, Semicond. Sci. Technol. 14 (1999) 642.
[22] R. Swanepoel, J. Phys. E: Sci. Instrum. 16 (1983) 1214.
[23] Jean-Marc Laurent, Agnès Smith, David S. Smith, Jean-Pierre Bonnet, Rafael Rodriguez Clemente, Thin Solid Films 29 (2) (1997) 145.
[24] P.V. Dhanaraj, N.P. Rajesh, J. kalyana Sundar, S. Natarajan, G. Vinihta, Mater. Chem. Phys. 129 (2011) 457.
[25] M. Birkholz, P.F. Fewster, C. Genzel, Thin film analysis by X-ray scattering, WILEY-VCH Verlag GmbH & Co, Weinheim, 2006.
[26] Dae-Sik Lee, Gi-Hong Rue, Jeun-Soo Huh, Soon-Don Choi, Duk-Dong Lee, Sens. Actuators, B 77 (2001) 90.
[27] Dai Hong Kim, Ji-Hwan Kwon, Miyoung Kim, Seong-Hyeon Hong, J. Cryst. Growth 322 (2011) 33.
[28] V.M. Kaganer, R. Köhler, M. Schmidbauer, R. Optiz, Phys. Rev. B 55 (3) (1997) 1793.
[29] P. Anandan, T. Saravanan, G. Parthipan, R. Mohan Kumar, G. Bhagavannarayana, G. Ravi, R. Jayavel, Solid State Sci. 13 (2011) 915.
[30] B. Riscob, Mohd. Shakir, J. Kalyana Sundar, S. Natarajan, M.A. Wahab, G. Bhagavannarayana, Spectrochim. Acta, Part A 78 (2011) 543.
[31] J.I. Owen, W. Zhang, D. Köhl, J. Hüpkes, J. Cryst. Growth 344 (2012) 12.
[32] V. Consonni, G. Rey, H. Roussel, D. Bellet, J. Appl. Phys. 111 (2012) 033523.
[33] D. Bélanger, J.P. Dodelet, B.A. Lombos, J.I. Dickson, J. Electrochem. Soc. 132 (1985) 1398.